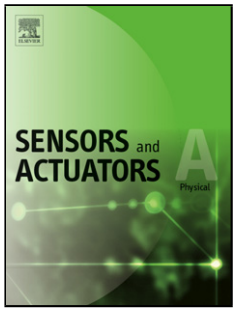

Title: Nanoscale radius-graded photonic crystal sensor arrays using interlaced and symmetrical resonant cavities for biosensing

Author: Qi Liu Huiping Tian Daquan Yang Jian Zhou Yi Yang Yuefeng Ji

PII: S0924-4247(14)00212-X
DOI: http://dx.doi.org/doi:10.1016/j.sna.2014.04.029
Reference: SNA 8770

To appear in: *Sensors and Actuators A*

Received date: 17-1-2014
Revised date: 18-4-2014
Accepted date: 19-4-2014

Please cite this article as: Q. Liu, H. Tian, D. Yang, J. Zhou, Y. Yang, Y. Ji, Nanoscale radius-graded photonic crystal sensor arrays using interlaced and symmetrical resonant cavities for biosensing, *Sensors and Actuators: A Physical* (2014), http://dx.doi.org/10.1016/j.sna.2014.04.029

Nanoscale radius-graded photonic crystal sensor arrays using interlaced and symmetrical resonant cavities for biosensing

Qi Liu,[1] Huiping Tian,[1] Daquan Yang,[1,2] Jian Zhou,[1] Yi Yang,[1] and Yuefeng Ji[1]

[1] The State Key Laboratory of Information Photonics and Optical Communications, School of Information and Telecommunication Engineering, Beijing University of Posts and Telecommunications, Beijing 100876, China

[2] School of Engineering and Applied Science, Harvard University, Cambridge, MA 02138, USA.

Corresponding author at: Beijing University of Posts and Telecommunications, P.O.BOX 90, #10 Xitucheng Road Haidian District, Beijing 100876, China. Tel.: +86 10 62282153.

Email addresses: hptian@bupt.edu.cn (H. Tian), jyf@bupt.edu.cn (Y. Ji).

Abstract: In this work, we propose radius-graded photonic crystal sensor arrays applied on nano-scale optical platform for label-free biosensing. Two L3 cavities and two H1 cavities are multiplexed and interlaced on both sides of a photonic crystal W1 waveguide on the radius-graded photonic crystal slab. The optical sensing characteristics of the nanocavity structure are predicted by three-dimensional finite difference time domain (3D-FDTD) simulation. In response to the refractive index change of air holes surrounding the cavities, four interlaced and symmetrical cavities are shown to independently shift their resonant wavelength without crosstalk. The simulation results demonstrate the refractive index sensitivity of sensor array varies from 66.67nm/RIU to 136.67nm/RIU corresponding to the number of functionalized air holes ranged from 4 to 21. This design makes different cavities multiplexed on both sides of waveguide possible. Meanwhile, the radius-graded photonic crystal with more symmetrical and interlaced cavities is better for large integration in the sensor arrays.

Keywords: Photonic crystal; Biosensor; Nanocavity; Waveguide; Integrated optics devices

1. Introduction

Since E. Yablonovitch and S. John firstly introduced the concept of photonic bandgap (PBG) in 1987 [1,2], photonic crystal (PhC) has attracted increasing attention in the past decades. Due to wide photonic bandgap and photon confinement ability, PhC devices are applied in many fields (e.g., photonic crystal filters [3-9], electro-optical modulators [10-12], switching devices [13,14], and delay devices [15]). Besides, PhC sensors seem to be very promising because of their ultracompact size, high spectral sensitivity and more suitable for monolithic integration. Thus, during the last decades, many PhC sensors for different sensing application have been demonstrated, such as stress sensing, humidity sensing, refractive index sensing, and biochemical sensing [16-23].

With the extensive research about photonic crystal sensors, ultra-high quality factor (Q) and high sensitivity can be achieved by using different kinds of structure such as microcavities [24,25], resonant rings and disks [26], slot waveguides [27,28], and heterostructures [29]. Photonic crystal biosensors detect analyte attached to the surface (surface-based sensing) or liquids filled into the holes around the PhC (bulk index sensing) via modulation of microcavity resonant wavelength. When the molecule exposed to a photonic crystal sensor is changed, the effective refractive index of the cavities will be changed. According to the Bragg diffraction principle [41], the resonant wavelength will shift along with the change of refractive index based on the same structure. So, a shift in the resonant wavelength peak will be caused in the transmission spectrum. Here the magnitude of the resonant wavelength shift is related to many factors, such as the number of functionalized holes, the spatial overlap of the mode with the analyte, the bandwidth of the photonic crystal structure, and so forth. Recently, nanoscale photonic crystal sensor array has drawn much

attention. The photonic crystal sensor arrays make detecting different analyte simultaneously on a single platform possible. Considering the multiple sensing performance and label-free biomolecular detection, photonic crystal sensor array is a better choice. Examples of such structures include that Yang et al. demonstrated a nanoscale photonic crystal sensor array on monolithic substrates using side-coupled resonant cavity arrays [30], S. Pal et al. designed a multiple nanocavity coupled device for error-corrected optical biosensing [31], and S. Mandal et al. proposed a nanoscale optofluidic sensor array based on a silicon waveguide with 1D (one dimensional) photonic crystal microcavity [32]. However, the drawbacks of these sensor arrays are that the scale is larger and fewer cavities could be allowed without crosstalk due to the limited bandwidth.

In this work, we propose a novel ultracompact interlaced and symmetrical radius-graded photonic crystal sensor array which can overcome the above limitations. The radius-graded photonic crystal structure has drawn much attention for some years. Works have mainly focused on the electromagnetic waves which propagate and transform along the graded structure. Due to its ability to efficiently control the propagation of light, the graded photonic crystal has been successfully applied as light bending, lens and photonic crystal demultiplexer [33-40]. In this paper, we firstly introduce the radius-graded structure to design photonic crystal sensor arrays. The device contains two pairs of interlaced and symmetrical resonant cavity arrays side-coupled to PhC W1 waveguide. Considering the easier and more accurately design in practical applications, we choose L3 cavity and H1 cavity as the resonant cavities [42-46]. By using three-dimensional finite-difference time-domain (3D-FDTD), we optimize the distance between the two cavities to minimize the size of photonic crystal sensor arrays without crosstalk. The sufficient simulation results reveal that the resonant wavelength of each micro-cavity shift linearly when the effective refractive index around the cavity change. The radius-graded photonic crystal sensor arrays can detect different kinds of analyte at the same time. In addition, the total sensor sensitivity is 113.34nm/RIU as the functionalized holes equal 12 (N=12). If we tuned the number of functionalized air holes, the sensitivity varies from 66.67 nm/RIU (N=4) to 136.67 nm/RIU (N=21). In addition, if we only use L3 cavity as the interlaced resonant cavity, the number of the microcavities could be added to six along with the direction of radius increasing in the platform. This means that the structure based on the nanoscale radius-graded photonic crystal platform is promising in the optical integrated circuit in the future.

2. Design of the radius-graded photonic crystal with interlaced micro-cavities

We examine the effect of adding different microcavities (H1 or L3) to the raidus-graded photonic crystal sensor arrays by performing 3D-FDTD simulations. The 3D illustration of our radius-graded photonic crystal sensor arrays structure with three interlaced H1 and L3 microcavities are shown in Fig. 1(a) and Fig. 1(b), respectively. The PhC devices have lattice constants (a) of 437nm with a slab thickness of 0.5a (220nm). Additionally, the structure in our paper is designed on a silicon slab (n_{si}=3.48) by arranging a triangular lattice of air holes. Moreover, the radius in our design is graded with r_1=0.28a, r_2=0.3a, r_3=0.32a. Using the radius-graded photonic crystal structure, we can easily achieve microcavity arrays in a platform.

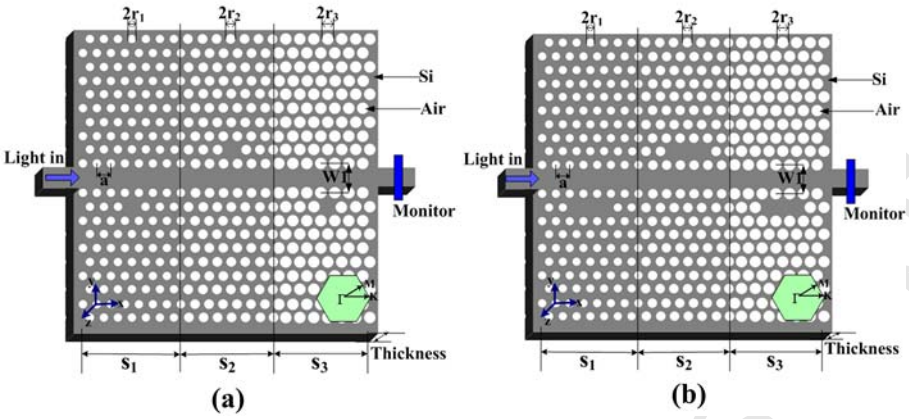

Fig. 1. 3D illustration of the graded photonic crystal with interlaced micro-cavities, where a=437nm, T=0.49a, r_1=0.28a, r_2=0.3a, r_3=0.32a. (a) structure for H1 cavity; (b) structure for L3 cavity.

As shown in Fig. 1, H1 and L3 cavities are regarded as the resonant cavities separately. H1 cavity represents removing one air hole, and L3 cavity stands for three air holes losing. Figure 1(a) shows the interlaced H1 microcavities, while Fig. 1(b) is the structure of L3 microcavities. The photonic crystal slab structure designed for biosensing is based on silicon, and consists of a 21×21 array of air holes in a triangular-lattice pattern. We use the TE polarized Gaussian-pulse source as the incident source. The simulations are performed by using Meep [30] to observe the steady state electric field and the transmission spectra. For improving accuracy in the simulation, FDTD analysis of photonic crystal structure is carried out with a mesh size of a/200 and time step of 0.025a/c, where a is the lattice constant. All the simulations are carried out with the same mesh size and time step for future comparable results. Since the boundary conditions at the spatial edges of the computational domain must be carefully considered. The simulation area in our paper is surrounded by one-spatial unit thick perfectly matched layer (PML), in which both electric and magnetic conductivities are introduced in such a way that the wave impedance remains constant, absorbing the energy without inducing reflections. Furthermore, the structural and simulation parameters keep the same except for cavities in the future research.

Since the graded photonic crystal has been applied as demultiplexer before [35], we firstly introduce this theory to sensor arrays. Figure 2 shows the band diagram of a W1 PhC slab waveguide by using plane wave expansion (PWE) method. From the simulation, we conclude the effective working frequency of the waveguide within the PBG is between 0.259($2\pi c/a$) and 0.308($2\pi c/a$). In figure 2(a) there are three different color lines (blue, green and black) which represent the mode under conditions of different radii. We focus on the even mode in our following research. We calculate that the blue line signifies the mode in r=0.28a, while the black one shows the mode when r is equal to 0.32a. It means that as the radius increasing the guided modes move to the higher frequency (blue line to the black line). Figure 2(b) shows the transmittance of the interlaced L3 cavities. The resonant frequency peaks of the L3 cavities all intersect with the even mode line in the band diagram. Because the radius-graded photonic crystal disrupts the periodicity, the transmission has some fluctuation on the edge of the bandgap. As seen, the radius-graded photonic crystal with three interlaced microcavities can generate three resonant wavelengths easily.

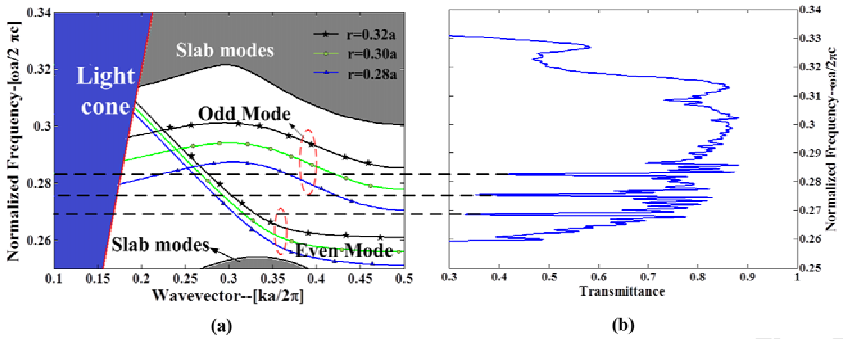

Fig.2. (a) Band diagram for a W1 waveguide. The blue, green and black lines represent the mode line in different radii. (b) The transmission spectra of the three L3 cavities structure. The dashed black lines are a guide for the eye.

As concluded the simulation about the structures pictured in figure 1, the refractive frequencies of three interlaced cavities separate clearly in the transmission spectra. To ensure every resonant frequency is introduced by the corresponding cavity, we research the three interlaced L3 cavities and H1 cavities respectively. As observed in Fig. 3(a) and Fig. 3(b), the three L3 cavities and three H1 cavities have perfect independence property. In addition, when designing the photonic crystal sensor arrays, not only the quality factor and sensitivity are crucial, but also the size of the structure is important. In order to decrease the size, we discuss the resonant frequency shift caused by the space between two cavities. Figure 3(c) illustrates the transmission spectra of different distances which affect the sensor array size directly. We can clearly point out that when the distance ranges from 10*a* down to 4*a*, the resonant frequencies are still at the same frequent points except that a few lobes have tiny deviation. What's more, the cavities interval has slightly effect on quality factor corresponding to the L=10*a*, 8*a*, 6*a*, 4*a*. And the fluctuation of quality factor based on different interval between cavities is so small that the impact on practical sensing research can be ignored. Thus, we can choose the appropriate distance for the future optimal design.

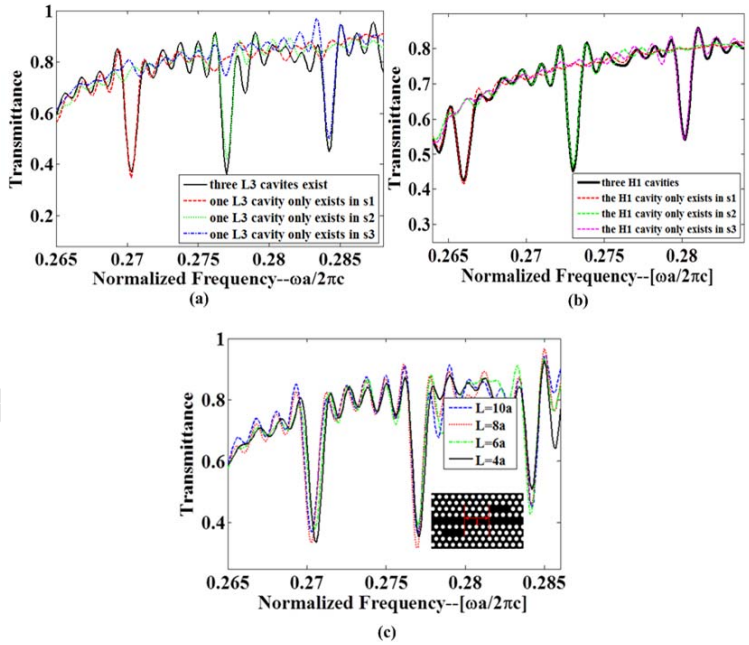

Fig. 3. (a) The black line represents the transmission spectra of three interlaced L3 cavities, while the dotted lines

signify the transmission of L3 cavity only exists in one sensor; (b) The transmission spectra of three interlaced H1 cavities marked in the black line, while the dotted lines signify the transmission of H1 cavity only exists in one sensor; (c) The transmission spectra of different distance (L=10*a*, 8*a*, 6*a*, 4*a*) between two interlaced L3 cavities based on radius-graded photonic crystal platform.

3. Design of photonic crystal sensor array with interlaced and symmetrical microcavities on the both sides of W1 waveguide

It is well recognized that the radius-graded photonic crystal could be applied in the small scale sensor arrays. For applications such as label-free biosensing and chemical detection, it should be noted that it is better when more sensor structures are designed on a nano-scale single platform. According to the research above [30,35], we discuss the interlaced and symmetrical microcavities on the both sides of W1 waveguide in order to detect different analytes on a single platform. As shown in Fig. 4, the radius-graded photonic crystal sensor arrays contain two H1 and L3 microcavities on the both sides of W1 waveguide. The parameters of the design are a=437nm, T=0.5a, r_1=0.28a, r_2=0.3a, respectively. With the 3D-FDTD simulation, the air holes radius around the cavities is slightly optimized to magnify the output transmittance. The radii of air holes marked blue (r_a) are 0.34a, and the red ones (r_b) are 0.4a.

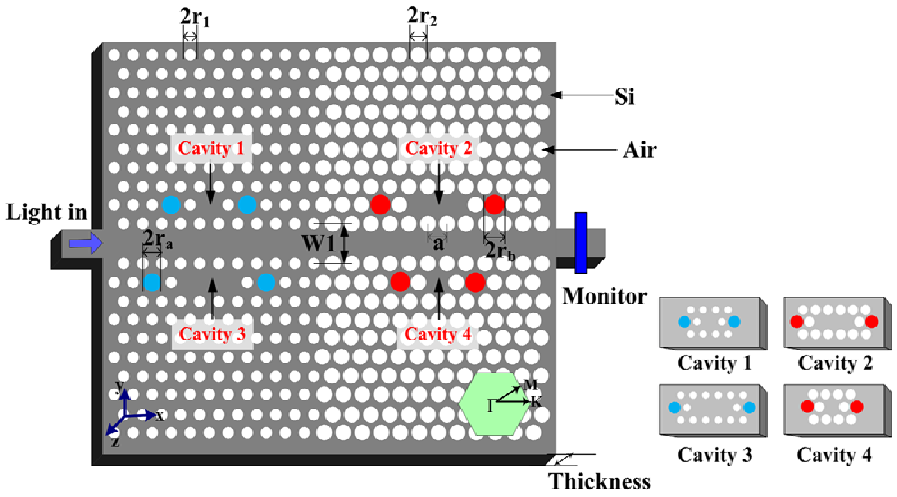

Fig. 4. The 3D illustration of symmetrical microcavities on the both sides of W1 waveguide. The design contains two L3 and H1 microcavities, where a=437nm, T=0.5a, r_1=0.28a, r_2=0.3a, r_a=0.34a, r_b=0.4a.

Figure 5 plots the light propagation profile in PhC and the output transmission spectra. The calculated resonant frequencies for the radius-graded photonic crystal sensor arrays are 0.2708($2\pi c/a$) (cavity3), 0.2778($2\pi c/a$) (cavity2), 0.282($2\pi c/a$) (cavity1), 0.2885($2\pi c/a$) (cavity4), respectively, corresponding to a lattice constant of 437nm. Examination of Figs. 5(a)-5(d) demonstrates the steady state electric field distribution (Ex) for the fundamental TE mode propagating in the x-y plane. Each cavity has a strong optical field so that the interlaced and symmetrical microcavities are sensitive corresponding to the change of refractive index. The output transmission spectrum for a radius-graded photonic crystal sensor device which consists of four resonant cavities is plotted in Fig. 5(e). We just magnify the radius of air holes that are around the four resonant cavities to optimize the cavities performance. The air holes marked in blue and red are r_a=0.34a and r_b=0.4a leading to an optimal device with high transmittance. In spite of the bandgap of our design being similar with that in [30], we apply the radius-graded photonic crystal structure to multiplex different kinds of cavities for biosensing.

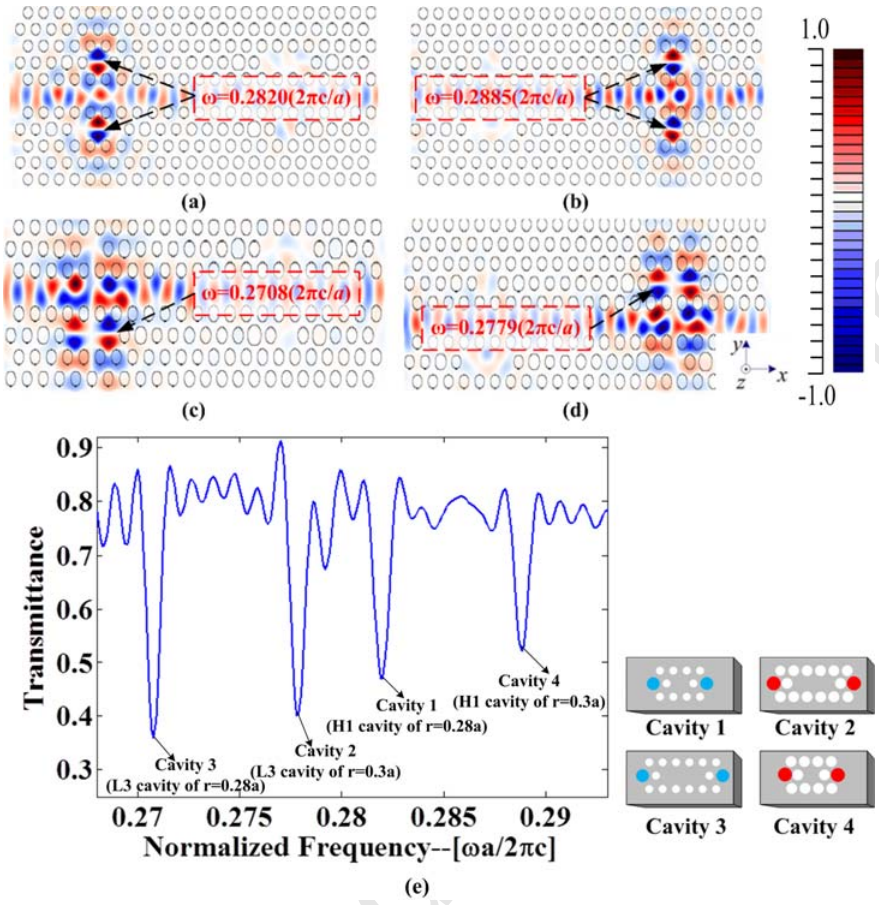

Fig. 5. The electric field distribution (*Ex*) for (a) cavity1 and cavity3, (b) cavity2 and cavity4, (c) cavity3, and (d) cavity2 in the *x*-*y* plane. (e) 3D-FDTD simulation showing the output transmission spectrum for a radius-graded photonic crystal sensor device (pictured in figure 4) consisting four interlaced and symmetrical cavities.

4. Simulation results and discussion

Based on the above optimal design, it is essential to note that the magnitude of the resonant wavelength shift is dependent on the combination of many factors such as the number of functionalized holes and the effective refractive index change. We assume that the holes around the cavities are totally injected with analyte. When a detection event occurs, the refractive index will change due to the detection targets infiltrated into the air holes around the resonant cavities. Here, we try different number of functionalized holes (N) nearby the resonant cavities in the photonic crystal sensor array illustrated in Figure 4 to study the relationship between the mass sensitivity and the number of functionalized holes. As can be seen in Fig. 6, simulations are performed in the case of the two functionalized holes (the two red holes marked in Fig. 6), four functionalized holes in the corner of the resonant cavities, eight functionalized holes, twelve functionalized holes and up to twenty-one functionalized holes. The mass sensitivity is defined as $\Delta\lambda/N$ where $\Delta\lambda$ is the resonant wavelength shift and N means the number of functionalized holes.

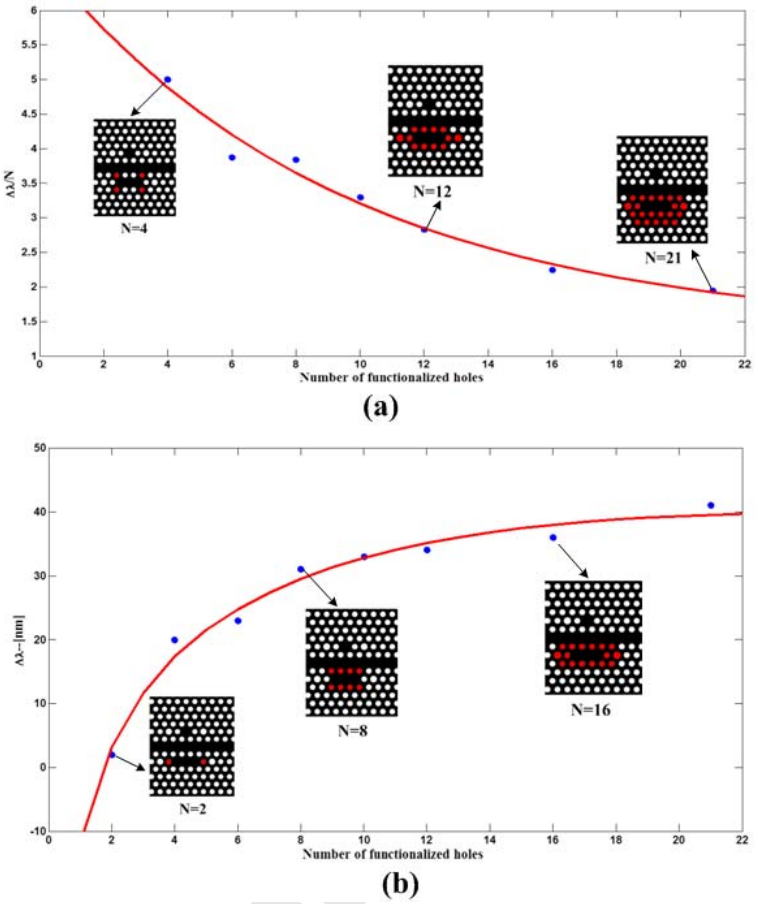

Fig. 6. (a) 3D-FDTD simulation showing the mass sensitivity of the design related to the number of functionalized holes. The blue circles illustrate the mass sensitivity, while the red curve shows an exponential fit; (b) Plot demonstrating the dependence of the resonant wavelength shift on the number of functionalized holes. The blue points indicate the data obtained by 3D-FDTD simulations. The red curve is a logarithmic fit curve of the form $a \times N + b \times log(cN) + m$, where *a, b, c* and *m* are the constants.

The blue points in Fig. 6(a) present the mass sensitivity (Δλ/N) in different cases. An exponential function which is $a+b\times e^{cN}$ can perfectly match the simulations, where the value of a, b and c are 1.3564, 5.4181, and -0.1074, respectively. We could see that targeting the inner holes around the resonant microcavity as the functionalized holes (N=4) allows the highest possible mass sensitivity for the device. Figure 6(b) illustrates the relationship between resonant wavelength shift (Δλ) and the number of functionalized holes (N). We use a logarithmic curve of the form $a\times N+b\times\log(cN)+m$ to fit our simulation results, where *a, b, c* and *m* are the arbitrary constants. The value of *a, b, c* and *m* are -0.9422, 23.053, 0.8114, and -6.083, respectively. As seen in Fig. 6, the resonant wavelength shift gets larger as the number of functionalized holes increases, while the mass sensitivity decreases. In the left area of N=12 (such as N=4, 8), the sensing element can realize higher mass sensitivity, but the resonant wavelength shift is lower. While in the right area of N=12 (such as N=16, 21), the sensing element can realize higher shift in resonant wavelength, but the mass sensitivity is lower. Thus, in our design we make a tradeoff between the wavelength shift and mass sensitivity and determine that the functionalized hole number is N=12 in the sensing element.

Through the design and discussion about the number of functionalized holes, a summary of

the resonant wavelength shift for the radius-graded photonic crystal sensor arrays is shown in Fig. 7. A series of 3D-FDTD simulations have been conducted to estimate the sensitivity of the sensor arrays illustrated in Figure 4. Figure 7(a) shows the transmission spectrum of the sensor arrays when two sensors are under variations in refractive index and others are not. The refractive index is set from 1.10 to 1.18 in the interval of 0.02. The shift only occurs with the functionalized sensors while others keep completely unchanged. We can see each resonant wavelength has the analogous linear shift due to the refractive index change. Figure 7(b) demonstrates the resonant wavelength shift of cavity2 when the target objects with different refractive indices are injected into the functionalized holes. When only one sensor is under the variations in refractive index, its resonant wavelength just shifts while other resonant wavelength dips are unaffected. We then further research the different cavities detect individually with kinds of molecules, and the results show that two or more cavities can detect different molecules at the same time. All these results represent that each sensor can work independently without crosstalk.

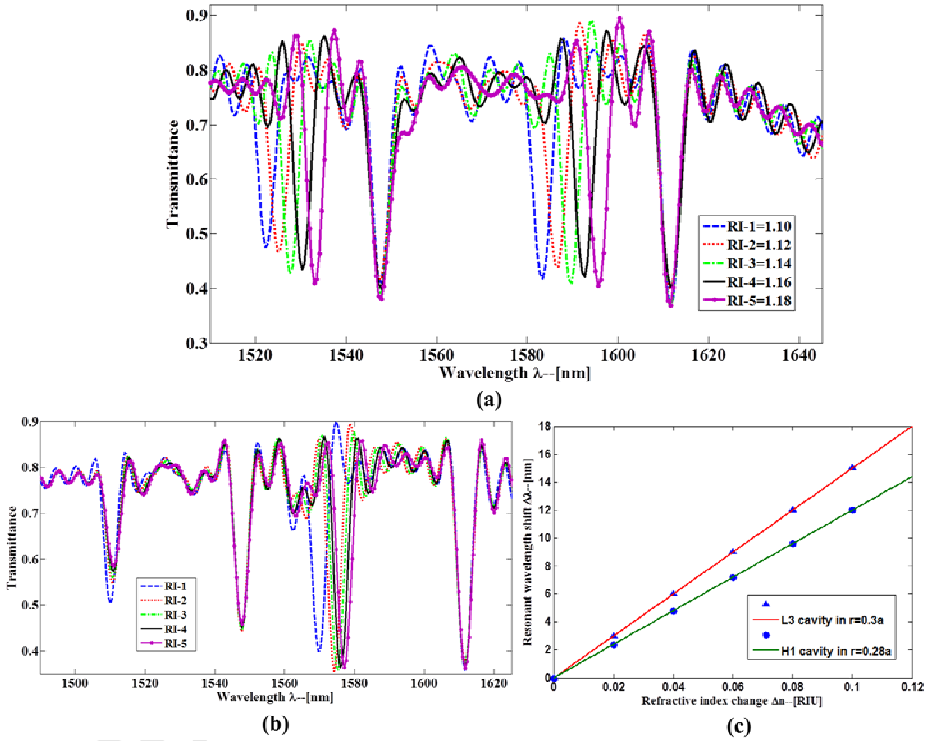

Fig. 7. (a) The transmission spectra of the sensor array while two microcavities are subjected to the change in refractive index. (b) The output transmission spectra of the structure when one of the sensors is under conditions of different refractive indices. (c) The resonant wavelength shift based on the refractive index changing for L3 and H1 cavities in different radii.

To investigate the sensitivity of the radius-graded photonic crystal sensor arrays, we perform a series of simulations based on different situations. According to the simulation results, we obtain the sensitivity shown in Fig. 7(c). The resonant wavelength shift is defined as $\Delta\lambda$ and the sensitivity of the sensors (S) can be expressed as

$$S = \frac{\Delta\lambda}{\Delta n} \tag{1}$$

Δn means the refractive index change. The sensitivities of the four resonant cavities are irregular as a whole due to the light not cloned well in the radius-graded shape. Moreover, the simulation results can prove the ability of light confinement in different cavities with different radius. It is easy to calculate the sensitivity of the radius-graded photonic crystal sensor arrays is close to 113.34nm/RIU when the number of targeting holes is 12. Besides, if all the air holes are applied as the functionalized holes, the calculated sensitivity can be up to 150nm/RIU. In a word, the sensitivity of the device can be varied from 66.67nm/RIU (N=4) to 150nm/RIU (N=all).

We then further research the detection limit of refractive index which is an important parameter in actual applications. The detection limit of refractive index changes (*DL*) can be expressed as follow [21]:

$$DL = \frac{\lambda}{SQ} \tag{2}$$

where λ represents the resonant wavelength, S is the sensitivity of the resonant cavity, and Q means the quality factor which is nearly 2000. In our proposed structure, the detection limit is about 6.5×10^{-3}.

In addition, the radius-graded photonic crystal structure is extensible. We also research the radius-graded photonic crystal sensor array using six interlaced L3 cavities as the resonant cavities achieve refractive index sensing without crosstalk. This structure that we designed in this paper allows multiplexing different resonant cavities on both sides of the photonic crystal waveguide on monolithic substrate. As a result, a large number of resonant microcavities can be multiplexed in an integrated optical platform with the radius-graded photonic crystal design.

5. Conclusion

In this paper we have proposed a novel nano-scale photonic crystal biosensor arrays platform with a three dimensional radius-graded photonic crystal structure. Firstly we research one kind of resonant cavities (L3 or H1 cavity) interlaced on the radius-graded photonic crystal slab. This basic design provides possibility to get more interlaced resonant cavities as sensor array in the optical integrated circuits. Then we multiplex two different resonant cavities on both sides of W1 waveguide in the radius-graded photonic crystal structure. As indicated from the simulation results, each resonant wavelength can shift independently without crosstalk corresponding to the change in refractive index. We demonstrate that the sensitivity of the design varies from 66.67nm/RIU (N=4) to 136.67nm/RIU (N=21) when the functionalized holes around the resonant microcavity are different. The architecture in this paper has the advantage of multiplexing different resonant cavities on both sides of waveguide with the radius-graded photonic crystal structure to get smaller scale of sensor array and realize multiple biosensing detection without crosstalk. It is more suitable for monolithic integration in actual design and applications.

Acknowledgments

This research was supported by NSFC (No.61372038), National 973 Program (No.2012CB315705), National 863 Program (No.2011AA010305), and Fund of State Key Laboratory of Information Photonics and Optical Communications (Beijing University of Posts and Telecommunications), P. R. China.

References

[1] E. Yablonovitch, “Inhibited spontaneous emission in solid-state physics and electronics,” Physical Review Letters 58 (20) (1987) 2059-2062.

[2] S. John, "Strong localization of photons in certain disordered dielectric super lattices," Physical Review Letters 58 (23) (1987) 2486-2489.
[3] G. Shen, H. Tian, D. Yang, and Y. Ji, "Integration of photonic crystal splitter and slow light waveguide for a microwave photonic filter," Photonic Journal 5 (4) (2013) 5501311.
[4] G. Shen, H. Tian, and Y. Ji, "Ultracompact ring resonator microwave photonic filters based on photonic crystal waveguides," Applied Optics 52 (6) (2013) 1218-1225.
[5] S. Feng and Y. Wang, "Unidirectional reciprocal wavelength filters based on the square-lattice photonic crystal structure with the rectangular defects," Optics Express 21 (1) (2013) 220-228.
[6] H. Takano, B. Song, T. Asano, and S. Noda, "Highly efficient multi-channel drop filter in a two-dimensional hetero photonic crystal," Optics Express 14 (8) (2006) 3491-3496.
[7] A. Q. Liu, E. H. Khoo, T. H. Cheng, E. P. Li, and J Li, "A frequency-selective circulator via mode coupling between surface waveguide and resonators," Applied Physics Letters 92 (2) (2008) 021119-021119-3.
[8] E. H. Khoo, T. H. Cheng, A. Q. Liu, J. Li and D. Pinjala, "Transmitting light efficiently on photonic crystal surface waveguide bend, " Applied Physics Letters 91 (17) (2007) 171109.
[9] E. H. Khoo, A. Q. Liu, X. M. Zhang, E. P. Li, J. Li, D. Pinjala, and B. S. Luk'yanchuk, "Exact step-coupling theory for mode-coupling behavior in geometrical variation photonic crystal waveguides," Physical Review B 80 (3) (2009) 035101.
[10] J. Wülbern, A. Petrov, and M. Eich, "Electro-optical modulator in a polymer-infiltrated silicon slotted photonic crystal waveguide heterostructure resonator," Optics Express 17 (1) (2009) 304-313.
[11] J. Brosi, C. Koos, L. Andreani, M. Waldow, J. Leuthold, and W. Freude, "High-speed low-voltage electro-optic modulator with a polymer-infiltrated silicon photonic crystal waveguide," Optics Express 16(6) (2008) 4177-4191.
[12] C. Lin, X. Wang, S. Chakravarty, B. Lee, W. Lai, J. Luo, A. Jen, and R. Chen, "Electro-optic polymer infiltrated silicon photonic crystal slot waveguide modulator with 23dB slow light enhancement," Applied Physics Letters 97 (9) (2010) 093304.
[13] M. Yanik, S. Fan, and M. Soljacic, "High-contrast all-optical bistable switching in photonic crystal microcavities," Applied Physics Letters 83 (14) (2003) 2739-2741.
[14] P. Barclay, K. Srinivasan, and O. Painter, "Nonlinear response of silicon photonic crystal microresonators excited via an integrated waveguide and fiber taper," Optics Express 13 (3) (2005) 801-820.
[15] M. F. Yanik and S. Fan, "Stopping light all optically," Physical Review Letters 92 (8) (2004) 083901.
[16] Y. Wang, H. Wang, Q. Xue, and W. Zheng, "Photonic crystal self-collimation sensor," Optics Express 20 (11) (2012) 12111-12118.
[17] D. Yang, H. Tian, N. Wu, Y. Yang, and Y. Ji, "Nanoscale torsion-free photonic crystal pressure sensor with ultra-high sensitivity based on side-coupled piston-type microcavity," Sensors and Actuators A 199 (2013) 30-36.
[18] H. Kurt, M. N. Erim, and N. Erim, "Various photonic crystal bio-sensor configurations based on optical surface modes," Sensors and Actuators B 165 (2012) 68-75.
[19] B. T. Tung, D. V. Dao, T. Ikeda, Y. Kanamori, K. Hane, and Susumu Sugiyama, "Investigation of strain sensing effect in modified single-defect photonic crystal nanocavity," Optics Express 19 (9) (2011) 8821-8829.
[20] J. L. Dominguez-Juarez, G. Kozyreff, and J. Martorell, "Whispering gallery microresonators for second harmonic light generation from a low number of small molecules," Nature Communications 2 (2011) 1-8.
[21] Y. Yang, D. Yang, H. Tian, and Y. Ji, "Photonic crystal stress sensor with high sensitivity in double directions based on shoulder-coupled slant nanocavity," Sensors and Actuators A 193 (2013) 149-154.
[22] Y. Liu, and H. Salemink, "Photonic crystal-based all-optical on-chip sensor," Optics Express 20 (18) (2012) 19912-19920.
[23] J. O. Grepstad, P. Kaspar, O. Solgaard, I. R. Johansen, and A. S. Sudbø, "Photonic-crystal membranes for optical detection of single nano-particles, designed for biosensor application," Optics Express 20 (7) (2012) 7954-7965.
[24] F. Ouerghi, F. AbdelMalek, S. Haxha, E. K. Akowuah, and H. Ademgil, "Design of multicavities on left-handed photonic-crystal-based chemical sensors," Journal Lightwave Technology 30 (20) (2012) 3288-3293.
[25] M. Notomi, E. Kuramochi, and T. Tanabe, "Large-scale arrays of ultrahigh-Q coupled nanocavities," Nature Photonics 12 (2) (2008) 741-747.
[26] X. Zhao, J. Tsai, H. Cai, X. Ji, J. Zhou, M. Bao, Y. Huang, D. Kwong, and A. Liu, "A nano-opto-mechanical pressure sensor via ring resonator," Optics Express 20 (2012) 8535-8542.
[27] M. Scullion, A. Falco, and T. Krauss, "Slotted photonic crystal cavities with integrated microfluidics for biosensing applications," Biosensors and Bioelectronics 27 (1) (2011) 101-105.
[28] A. Falco, L. Faolain, and T. Krauss, "Chemical sensing in slotted photonic crystal heterostructure cavities," Applied Physics Letters 94 (6) (2009) 063503.
[29] B. Song, S. Noda, T. Asano, and Y.Akahane, "Ultra-high-Q photonic double-heterostructure nanocavity," Nature Materials 4 (3) (2005) 207-210.
[30] D. Yang, H. Tian, and Y. Ji, "Nanoscale photonic crystal sensor arrays on monolithic substrates using side-coupled resonant cavity arrays," Optics Express 19 (21) (2011) 20023-20034.
[31] S. Pal, E. Guillermain, R. Sriram, B. Miller, and P. Fauchet, "Silicon photonic crystal nanocavity-coupled waveguides for error-corrected optical biosensing," Biosensors and Bioelectronics 26 (10) (2011) 4024-4031.
[32] S. Mandal and D. Erickson, "Nanoscale opto-fluidic sensor arrays," Optics Express 16 (3) (2008) 1623-1631.

[33] E. Centeno and D. Cassagne, "Graded photonic crystals," Optics Letters 30 (17) (2005) 2278-2280.
[34] K. Ren and X. Ren, "Controlling light transport by using a graded photonic crystal," Applied Optics 50 (15) (2011) 2152-2157.
[35] K. Do, X. Roux, D. Marris-Morini, L. Vivien, and E. Cassan, "Experimental demonstration of light bending at optical frequencies using a non-homogenizable graded photonic crystal," Optics Express 20 (4) (2012) 4776-4783.
[36] B. Vasi´c, G. Isi´c, R. Gaji´c, and K. Hingerl, "Controlling electromagnetic fields with graded photonic crystals in metamaterial regime," Optics Express 18 (19) (2010) 20321-20333.
[37] F. Gaufillet, É. Akmansoy, "Graded photonic crystals for graded index lens," Optics Communications 285 (10) (2012) 2638–2641.
[38] Q. Wu, J. M. Gibbons, and W. Park, "Graded negative index lens by photonic crystals," Optics Express 16 (21) (2008) 16941-16949.
[39] E. Cassan, K. Do, C. Caer, D. M. Morini, and L. Vivien, "Short-Wavelength light propagation in graded photonic crystals," Journal of Lightwave Technology 29 (13) (2011) 1937-1943.
[40] H. T. Chien and C. C. Chen, "Focusing of electromagnetic waves by periodic arrays of air holes with gradually varying radii," Optics Express 14 (22) (2006) 10759-10764.
[41] J. H. Holtz and S. A. Asher, "Polymerized colloidal crystal hydrogel films as intelligent chemical sensing materials," Nature 389 (6653) (1997) 829-832.
[42] I. J. Luxmoore, E. D. Ahmadi, B. J. Luxmoore, N. A. Wasley, A. I. Tartakovskii, M. Hugues, M. S. Skolnick, and A. M. Fox, "Restoring mode degeneracy in H1 photonic crystal cavities by uniaxial strain tuning," Applied Physics Letters 100 (12) (2012) 121116.
[43] S. Olyaee and S. Najafgholinezhad, "Computational study of a label-free biosensor based on a photonic crystal nanocavity resonator," Applied Optics 52 (29) (2013) 7206-7213.
[44] Y. Akahane, T. Asano, B. Song, and S. Noda, "High-Q photonic nanocavity in a two-dimensional photonic crystal," Nature 425 (2013) 944-947.
[45] B. T. Tung, D. V. Dao, T. Ikeda, Y. Kanamori, K. Hane, and S. Sugiyama, "Investigation of strain sensing effect in modified single-defect photonic crystal nanocavity," Optics Express 19 (9) (2011) 8821-8829.
[46] W. Lai, S. Chakravarty, Y. Zou, and R. T. Chen, "Silicon nano-membrane based photonic crystal microcavities for high sensitivity bio-sensing," Optics Letters 37 (7) (2012) 1208-1210.

Biographies：

Qi Liu received the bachelor's degree of Communication Engineering from Shandong University in 2012. She is currently a master candidate in the State Key Laboratory of Information Photonics and Optical Communications, Beijing University of Posts and Telecommunications (BUPT), Beijing, P.R. China. Her research now focuses on the area of photonic crystals and sensors.

Huiping Tian received the BS and PhD degrees from Shanxi University, Shanxi, China, in 1998 and 2003, respectively. Now she is a professor in the School of Information and Communication Engineering, Beijing University of Posts and Telecommunications (BUPT), Beijing, China. Her research interests are focused on the area of ultra-short and ultra-fast process in the transmission of optics, photonic crystals and broadband information networking.

Daquan Yang received the bachelor's degree of Electronic Information Science and Technology from JiNan University in 2009. He is currently a PhD candidate in the State Key Laboratory of Information Photonics and Optical Communications, Beijing University of Posts and Telecommunications (BUPT), Beijing, P.R. China. His research now focuses on the area of photonic crystals and optical communication.

Jian Zhou received the bachelor's degree of Electronic Information Science and Technology from Nanjing University of Posts and Telecommunications (NUPT) in 2012. He is currently a master candidate in the State Key Laboratory of Information Photonics and Optical Communications, Beijing University of Posts and Telecommunications (BUPT), Beijing, PR China. His research now focuses on the area of photonic crystals and sensors.

Yi Yang received the bachelor's degree of Electronic Information Engineering from Beijing University of Posts and Telecommunications (BUPT) in 2011. He is currently a master candidate in the State Key Laboratory of Information Photonics and Optical Communications, Beijing University of Posts and Telecommunications (BUPT), Beijing, P.R. China. His research now focuses on the area of photonic crystals and sensors.

Yuefeng Ji received the PhD degree from Beijing University of Posts and Telecommunications (BUPT), Beijing, China. Now he is a professor in BUPT. His research interests are primarily in the area of broadband communication networks and optical communications, with emphasis on key theory, realization of technology and applications.

Highlights

This paper firstly proposes a nanoscale photonic crystal sensor arrays using radius-graded structure for biosensing. The sensor arrays can detect different molecules at the same time without crosstalk. The device is novel with four symmetrical nanocavities interlaced-coupled along the W1 waveguide which can largely decrease the sensing footprint. The radius-graded photonic crystal is more suitable for monolithic integration in actual design and applications.